Severely defor stainless steel

The microstructure of 8 μm diameter wire produced by the severe deformation of 316L austenitic stainless steel has been examined using transmission electron microscopy and X-ray diffraction. The deformation imparted amounts to a true strain of 6.3. Data from previous studies on the strain-induced transformation of this steel have been combined with new results to show that true strains greater than two are required in order to observe mechanical stabilisation, ie, the cessation of martensitic transformation when the martensite/austenite interfaces are unable to propagate through the dislocation debris created in the austenite.

Textiles woven using stainless steel threads have applications requiring softness, flexibility, abrasion resistance and the ability to serve at temperatures as high as 650 °C. The woven fabrics are generally made using 316L austenitic stainless steel threads and are used, for example, to make mold covers for automotive windshield manufacture and generally in glass manufacturing processes. Conveyor belts used in the glass industries sometimes have to be heated in order to avoid thermally shocking hot components, whereas those made using stainless steel fabrics can be used without preheat.

The stainless steel thread is made by drawing 190 μm fully-annealed stock to a final diameter of 8 μm, without any intermediate heat-treatment. A bundle of the thread together with an image of a single, slender fibre are illustrated in Figure 1.

Previous studies of deformed 316L have indicated that rolling deformation induces the transformation of the austenite into α martensite, with the quantity of martensite increasing disproportionately with plastic strain. [1,2] However, the levels of plastic strain utilised in previous work are dwarfed by that used to produce the stainless steel thread, where the true strain amounts to about 6.3. This is interesting from a metallurgical point of view because theory indicates that whereas the defects created by deformation increase the number density of nucleation sites and hence promote nucleation, the movement of the martensite-austenite (α/γ) interface is obstructed by the defects. When the strain becomes sufficiently large, it becomes impossible for the interfaces to move, causing the transformation to halt. The phenomenon arises because the α/γ interface must be glissile and is known as mechanical stabilization. [3,4,5,6,7,8,9,10,11,12]

Table 1. The chemical composition of the steel used, wt%

C	Si	Cr	Ni	Mn	Mo	P	S	N
0.01	0.75	17.1	11.97	0.53	1.99	0.006	0.001	0.046

med austenitic wire

AUTHORS:

Han-Shen Wang, J. R. Yang
National Taiwan University
Materials Science and Engineering
1 Rosevelt Road, Section 4, Taipei, Taiwan ROC (106)
Web: www.mse.ntu.edu.tw/homepage_english/ntumse.htm

H. K. D. H. Bhadeshia
University of Cambridge, Materials Science and Metallurgy
Pembroke Street, Cambridge CB2 3QZ, UK
Web: www.msm.cam.ac.uk/phase-trans

The purpose of the present work was therefore to understand the structure of the 316L wire in its heavily deformed state and to interpret the results to see whether mechanical stabilisation sets in at the extraordinarily large strains involved.

Experimental Procedure

Stainless steel (316L) wires with 190 μm diameter in the annealed state are used as the starting material in the manufacturing process. The chemical composition is given in Table 1. The actual annealing temperature is proprietary information but it is in excess of 800 °C.

The diameter of the starting 190 μm wires is reduced to 8 μm by cold-drawing, without any intermediate annealing. The true strain is thus 6.3 and results in the partial transformation of the austenite into ferromagnetic martensite.

The method by which specimens were prepared from this fine wire, for transmission electron microscopy (TEM) is illustrated in Figure 2. The wire is stretched and mounted between silicon chips using an epoxy adhesive (EpoxyBond 110, Allied High Tech Products, Inc.) and the assembly cured at 150 °C for 15 minutes before cooling to ambient temperature. The bonded assembly was then affixed to a glass plate using wax (Crystal bond 590, Aremco), heated to 150 °C and then cooled to ambient temperature. The specimen-glass set is then thinned by abrasion on silicon carbide papers with 800 and 4000-grit (Figures 2b and 2c, to

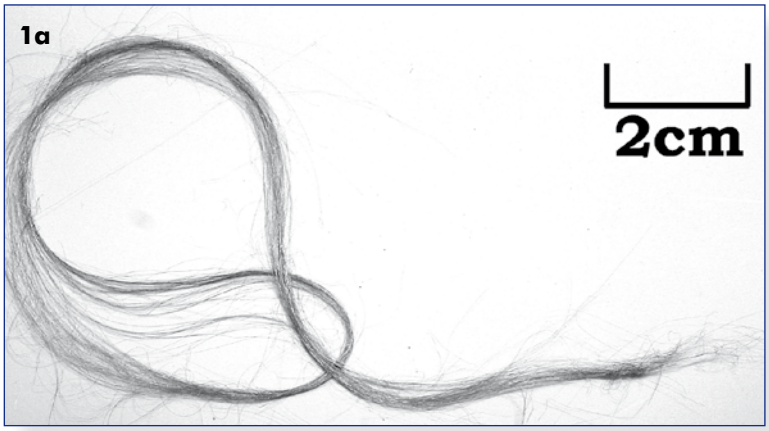

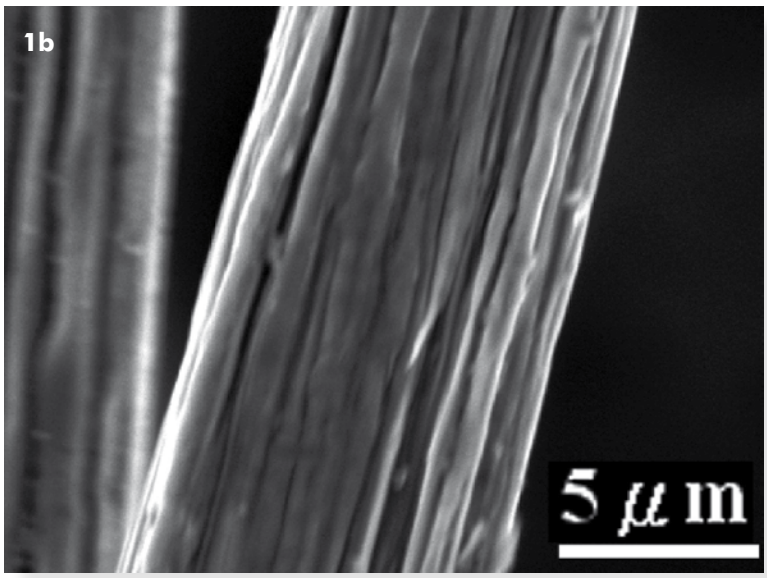

Figure 1a (above): An illustration of a stainless steel thread bundle in its final form; Figure 1b (below): Scanning electron micrograph of the individual fibre showing the rough surface resulting from the drawing operation

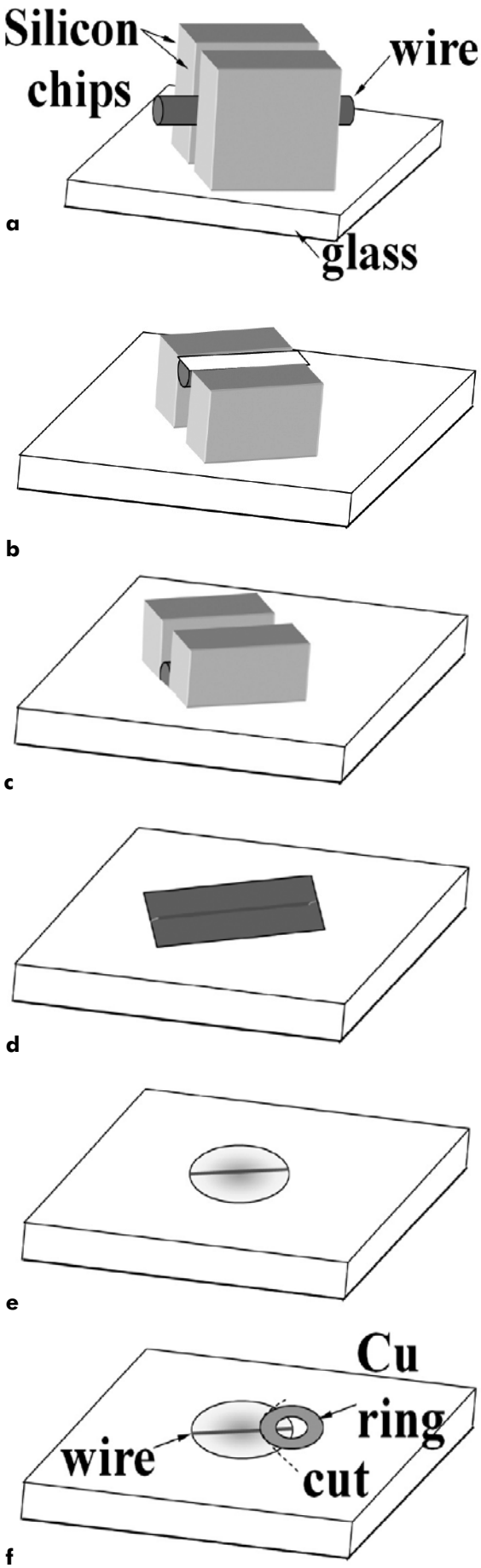

Figure 2 a-f (left): Illustration of the process for the preparation of a thin foil from the 8 μm diameter stainless steel wire

produce the section illustrated in Figure 2d. The transmitted colour of the silicon ranges from deep red to red for thicknesses of 5 to 10μ respectively, permitting the thickness to be monitored.[13] After the wire emerges from the thinned wafer, the polishing is continued using diamond with particles sizes of 1, 0.5, and 0.1μm, finishing with 0.06 μm silica wheel.

Interference fringes become visible when the thickness is <2 μm with a yellow transmission colour. The observation of fringes marks the perforation of the foil which is then mounted onto a copper grid (Figure 2), and moved into a plasma cleaner for drying and cleaning for transmission electron microscopy. Ion milling was not used in order to avoid the damage of ion bombardment. The foils were examined using JEM 100CX and 2000EX transmission electron microscopes operating at 100 and 200 kV respectively.

The volume fractions of martensite and austenite were determined by using a Brucker AXS Type B8 Advance X-ray diffractometer with the X-ray source of Cu-K α = 1.541Å) operating at 30 kV and 20 mA. The phase fractions were determined taking into account the integrated intensities of (111), (200) and (220) austenite peaks, and of (110), (200), (211) martensite in order to mitigate the effects of crystallographic texture.[14]

Microscopy

The initial microstructure of 190 μm diameter wire is presented in Figure 3; there are equiaxed austenite grains of size of about 2 μm peppered with annealing twins. Although the grains are equiaxed in this annealed sample, Figure 3 reveals a high dislocation density. It is believed that this is an artifact of the foil preparation technique, which involves grinding and polishing until perforation is achieved.

Figure 4 shows transmission electron micrographs taken from the transverse and longitudinal sections of the 8μm diameter wire. The transverse section actually has a very fine-grained structure (Figure 4a).

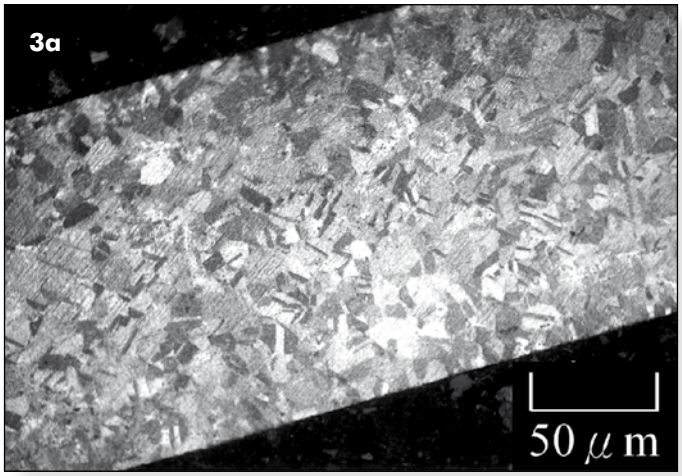

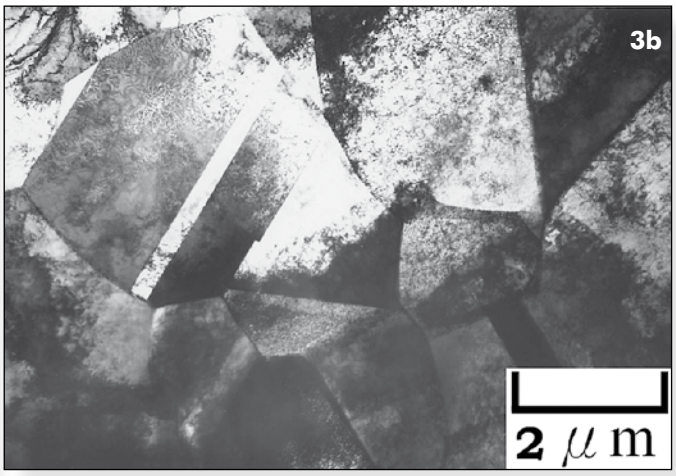

Figure 3 (above): 190 μ diameter wire. (a) Longitudinal section illustrating the equiaxed grain structure; (b) Longitudinal section transmission electron micrograph of the grain structure

The longitudinal section naturally shows extremely elongated grains due to the deformation. The combination of micrographs shows that the grains are roughly in the form of prisms elongated in the drawing direction but equiaxed in the cross-section.

Both the electron diffraction patterns in Figure 4 are taken using a 2 μm diameter selected area aperture in order to enclose many grains. The electron diffraction pattern from the transverse section (normal to the drawing direction) shows clearly that the

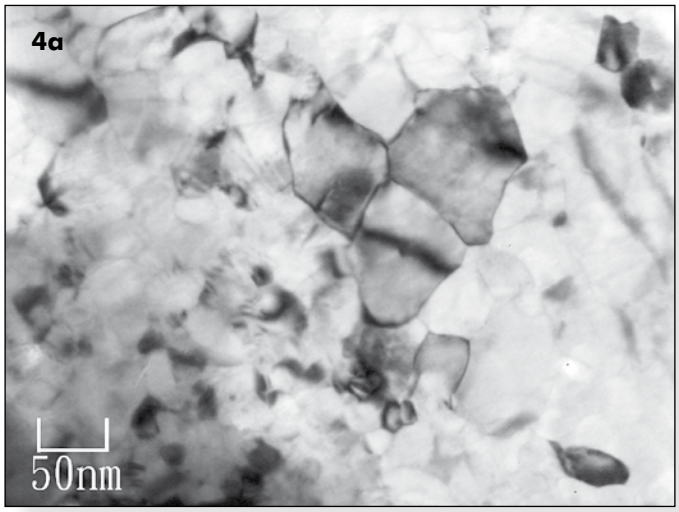

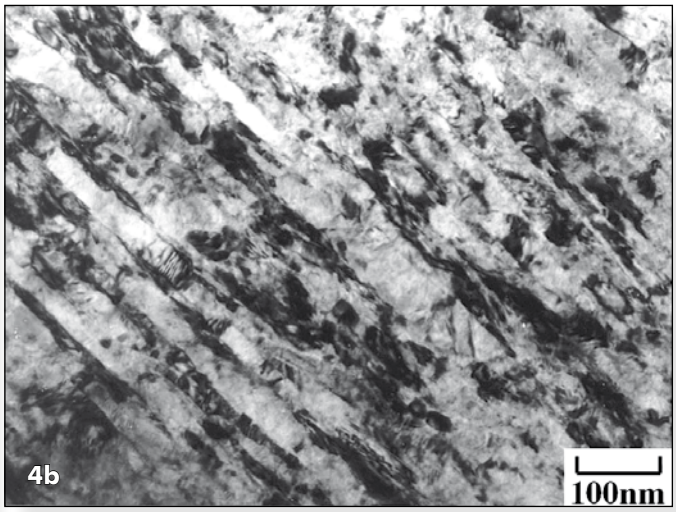

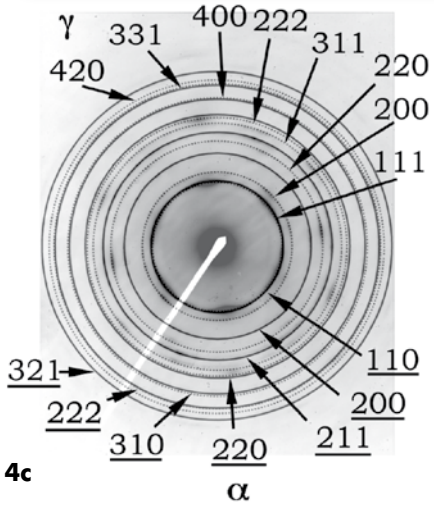

Figure 4. 8 μm diameter wire: (a) TEM image, transverse section; (b) TEM image, longitudinal section; (c) Electron diffraction pattern from transverse section; (d) Electron diffraction pattern from longitudinal section

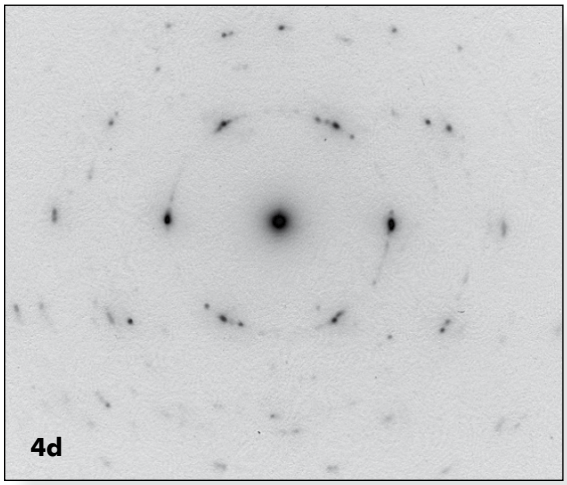

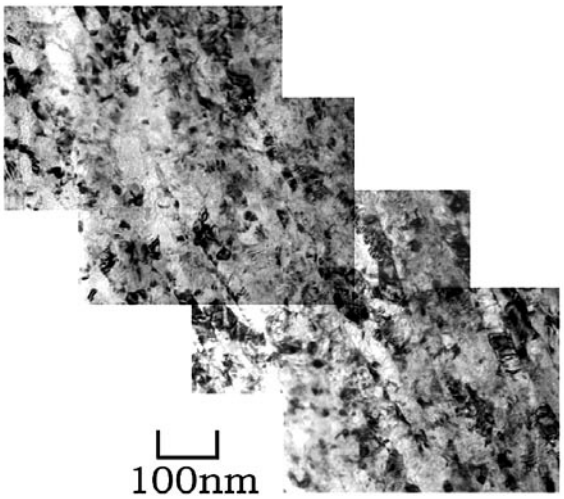

5a) Brigh-field image

Figure 5 a-c: Montage of transmission electron micrographs of longitudinal section of wire

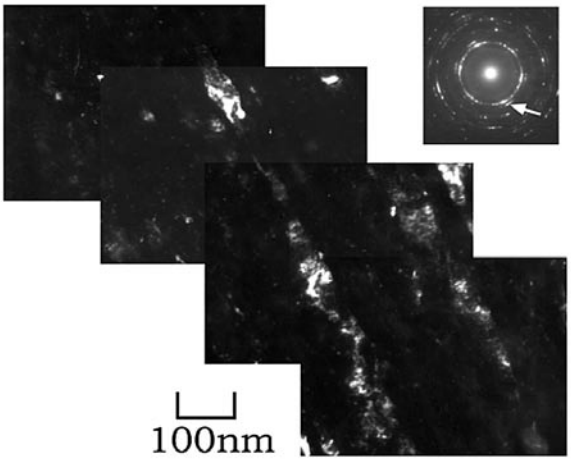

5b) Dark-field image of austenite using a 200γ reflection

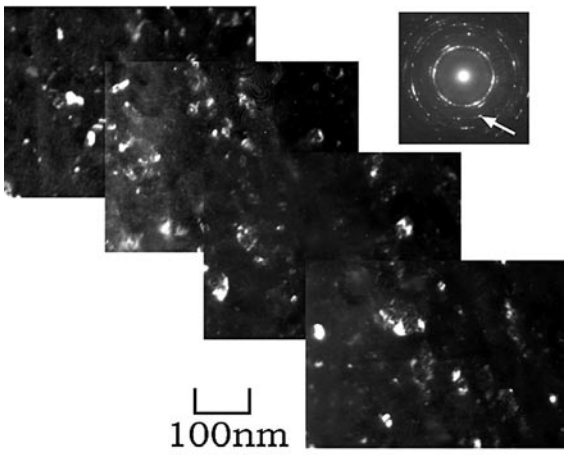

5c) Dark-field image of martensite using a 200α reflection

material is a mixture of austenite and martensite Figure 4c. The pattern is in the form of rings, consistent with many crystallographic orientations generated by rotation about the longitudinal axis. Not surprisingly, the pattern taken from the longitudinal section, which contains the drawing direction, shows strong crystallographic texture.

Because of the severity of deformation, it is not easy to deduce the individual morphologies of austenite and martensite from the micrographs in Figure 5. As will be seen later, the martensite appears to form at the early stages of straining and hence becomes deformed as the drawing operation continues. It is not surprising therefore that both the austenite and martensite appear as if they consist of classical dislocation cells. The austenite, being the matrix phase, shows greater continuity whereas the martensite presumably forms in many variants and hence appears to be in the form of discrete islands.

Phase Fractions

Consistent with the transmission microscopy, X-ray analysis of the 190 µm wire indicated that it is fully austenitic, Figure 6a. The cold reduction by a true strain of 6.3 to the 8 µm thread, resulted in the formation of about 57% of α-martensite in the microstructure, Figure 6b. The diffraction peaks from the deformed samples are broader, reflecting the influence of the strains locked in the microstructure.

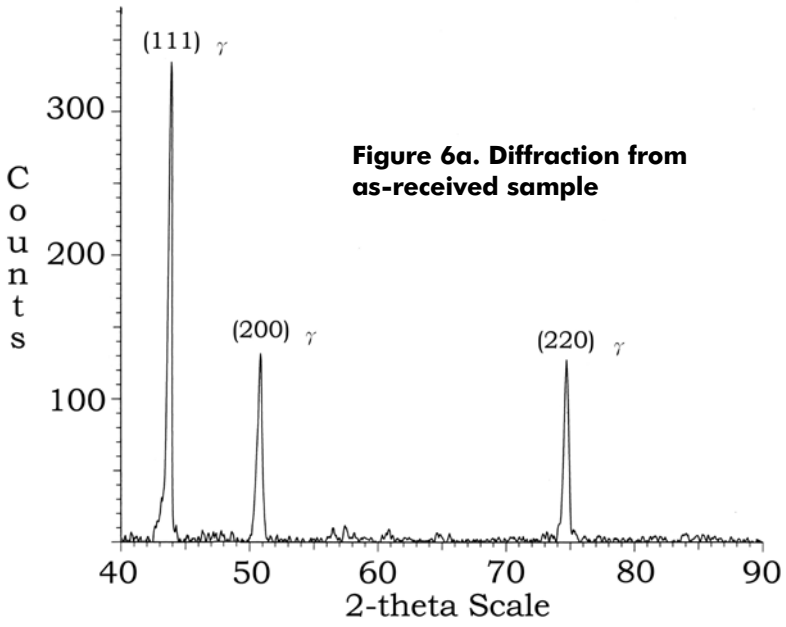

Figure 6a. Diffraction from as-received sample

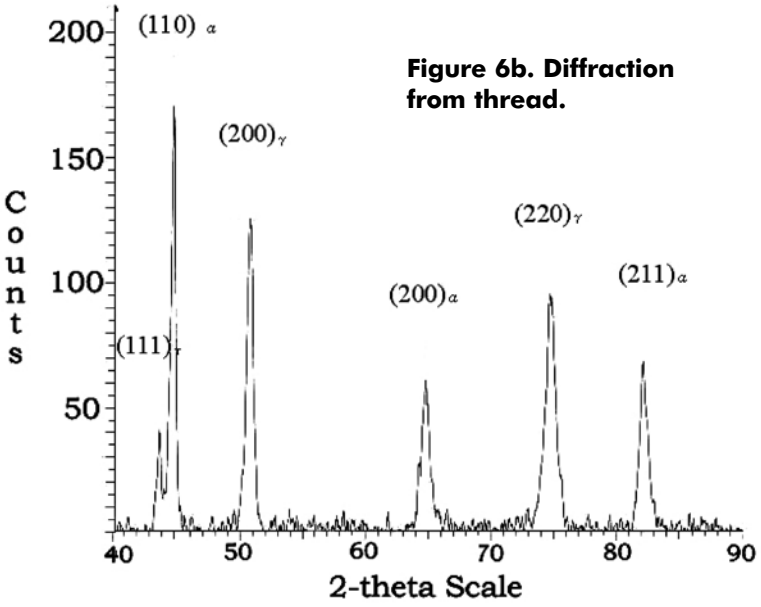

Figure 6b. Diffraction from thread.

It is well-known that stainless steels such as 316L are in a metastable state when they are fully austenitic. Equilibrium requires the presence of ferrite at all temperatures. This is illustrated in Figure 7, where calculated equilibrium data are presented for a variety of states. The calculations were conducted using MTDATA,[15] which is software capable of accessing thermodynamic data and estimating the equilibrium phase fractions and their chemical compositions as a function of a specified steel composition, set of possible phases, temperature, pressure etc.; the SGTE database was used in the present work.

It is also possible to do calculations involving constrained equilibria. Paraequilibrium is a state in which the substitutional atoms are cofigurationally frozen; the transformation of austenite to ferrite in these circumstances constrains the substitutional solute to iron atom ratio to be constant everywhere, whilst carbon partitions to achieve a uniform chemical potential subject to this constraint. It is often the case in steels that paraequilibrium prevails because the mobility of interstitial solutes such as carbon is so much greater than that of atoms in substitutional sites. Figure 7 shows that 316L can become fully austenitic at temperatures above 863 K when only paraequilibrium transformation is allowed.

Two further cases are illustrated in Figure 7, the first for equilibrium in which only ferrite and austenite are allowed to exist, and the second for the case where cementite and M23C6 are also allowed to exist. It is clear that neither case can explain the fully austenitic state of the 190 μm wire. Indeed, equilibrium involving the carbides requires that the ferrite contains huge chromium concentrations at low temperatures , e.g. in excess of 80 wt% for T < 863 K. Since this Cr-rich ferrite is not found in practice, it is safe to assume that an equilibrium state based on ferrite, austenite and carbides is not representative of commercial 316L.

The corresponding α + γ equilibrium calculations can also be dismissed on the grounds that they suggest an excessive quantity of ferrite in the microstructure prior to deformation, Figure 7.

Since the 190 μm wire is found to be fully austenitic, it must be concluded that the paraequilibrium calculations best represent the initial state of the wire. This in turn implies that the processing during its manufacture is sufficiently rapid to prevent the diffusion of substitutional solutes, thus allowing the material to be essentially austenitic in its underformed state. The initial wire is certainly not at equilibrium since considerable quantities of ferrite are then expected in the microstructure but not found in practice.

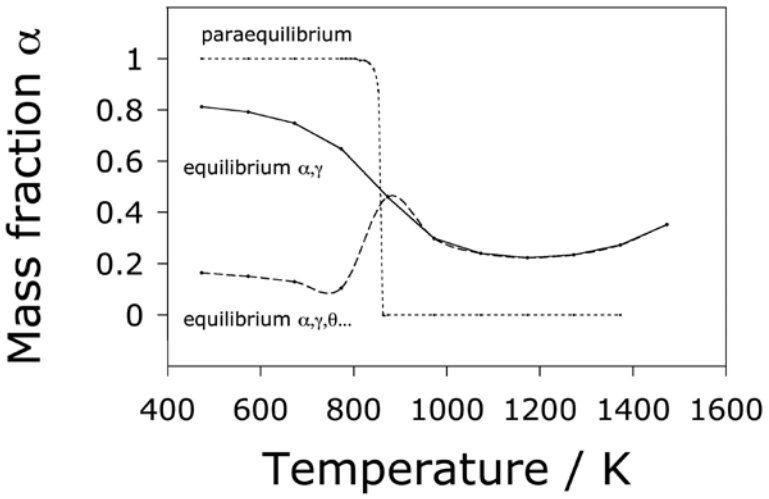

Figure 7 (above): Calculated ferrite phase fractions for α + γ paraequilibrium, α + γ equilibrium, α + γ + carbides equilibrium

Evidence for Mechanical Stabilisation

Martensitic transformation occurs without diffusion, and given the very low carbon concentration in the steel, this is, from a composition point of view, equivalent to saying that it occurs with paraequilibrium. It follows from paraequilibrium that only ferrite is the stable at ambient temperature. It should therefore be possible in principle to completely transform the austenite into martensite.

We have used a neural network technique[16,17] in order to treat the combined dataset and discover the relationship between the martensite fraction and true strain. This method has considerable advantages over normal curve-fitting, summarised as follows, with the details described in[16,17]:

- The fitting function is not a prior assumption as in normal regression analysis but is an outcome of the method.
- The method also provides a modelling uncertainty which indicates the ability of the model to generalise, that is, to make predictions outside of the range of experimental data. The error bar associated with this depends on the position in the input domain where calculations are done. If the calculations are done using inputs where knowledge is sparse then the indicated uncertainty is large.

Table 2: The amount of martensite as a function of true strain in 316L (data from [1,2])

Strain	0.148	0.195	0.278	0.420	0.470	0.995		
% martensite	4.0	4.2	4.5	8.0	10.0	14.0		

The fact that we obtain only 57% martensite following severe deformation is proof for the onset of mechanical stabilisation. As explained in the introduction, the α/γ interface contains glissile dislocations whose motion is hindered or prevented by the presence of defects in the austenite. The retardation of martensitic transformation from plastically deformed austenite has been observed in many systems.[3,4,5,6,7,8,9,10,11,12] On the other hand, as Table 2 shows, the data for 316L contradict this statement since they show an ever increasing martensite content up to true strains of about 1, with the rate of martensite formation rising with strain. This contrasts with mechanical stabilisation reported in 410 stainless steel after a strain of just 0.4.[11]

The present work provides an additional point in the experimental database for 316L, that the amount of martensite for a true strain of 6.3 is 57%. This assumes that the published data[1,2] – which are for rolling deformation – can be compared against our datum which is for wire drawing. This may be justified since it is the operation of multiple slip systems and their intersections which stimulate martensite [2], and multiple slip is inherent in both rolling and drawing.

Figure 8 shows the predicted behaviour alongside the experimental data. It is important to know that the central curve is deduced by the network using procedures which avoid overfitting (fitting to noise in the data); it is not imposed on the data as in normal regression analysis. The two bounding curves represent the modelling uncertainty. It is interesting that the modelling uncertainty is not excessive even in the region where there are no experimental data. This means that the form of the curve is reasonable - furthermore, the shape is as expected from mechanical stabilisation. There is a region at low strains where martensitic transformation is clearly accelerated by plastic deformation. It is predicted that the austenite becomes mechanically stabilised at a true strain of about 2. This explains why only 57% martensite is observed with the drawing strain of 6.3, even though the thermodynamic analysis indicates that it should in principle be

Acknowledgement: The authors are grateful to the National Science Foundation (Taiwan, ROC) and the Royal Society (UK) for partly funding this research.

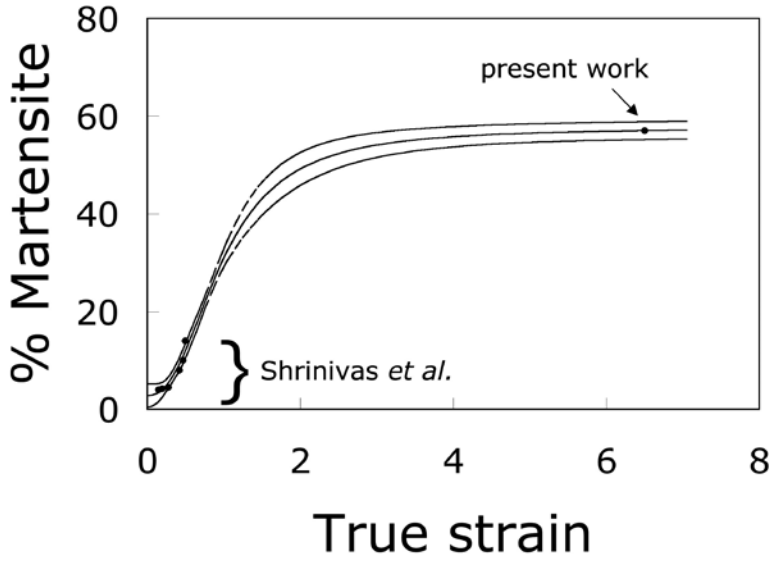

Figure 8 (above): Experimental data (points) and a neural network model (solid curve). The bounding curves represent ±1σ modelling uncertainties

possible to obtain fully martensitic samples at ambient temperature.

A further implication of mechanical stabilisation at a true strain $\varepsilon = 2$ is that any strain beyond 2 will simply deform existing martensite and austenite. This is why the observed morphology of martensite is like austenite, consistent with a deformed state.

Finally, it is worth considering whether the material undergoes dynamic recrystallisation during the course of deformation. The drawing operation is carried out at room temperature and very high speeds. It is unlikely therefore that recrystallisation, which requires diffusion, features in the process. The fact that the material is a two-phase mixture also would interfere with any recrystallisation process.

Conclusions

Stainless steel (316L) thread reduced by drawing to 8 μm diameter has a microstructure consisting of strain-induced martensite and austenite. The grain structure is strongly textured and in three dimensions is approximated by space-filling prisms elongated along the drawing direction.

It has been demonstrated that although the austenite can under paraequilibrium conditions transform completely into martensite, it is unable to do so in spite of huge strains, because of the onset of mechanical stabilisation. The stabilisation probably occurs at a strain of 2, so that the subsequent drawing simply deforms the existing mixture of martensite and austenite.

The work suggests further experiments, in which the evolution of martensite is studied in the range $\varepsilon = 1.5$ to 3. It would also be interesting to study the evolution of microstructure when the deformation is carried out at a lower temperature where the driving force for transformation is greater; the onset of mechanical stabilisation should then occur at a greater strain.

Bibliography

1. S. K. Varma, J. Kalyanam, L. E. Murr, **Journal of Materials Science Letters** 13 (1994) 107-111.
2. V. Shrinivas, S. K. Varma and L. E. Murr, **Metall. and Mater.** Trans. A 26A (1995) 661-671.
3. J. F. Breedis and W. D. Robertson, **Acta Metallurgica** 11 (1963) 547-559.
4. R. Lagneborg, **Acta Metallurgica** 12 (1964) 823-843.
5. J. R. Strife, M. J. Carr and G. S. Ansell, **Metallurgical Transactions** A 8A (1977) 1471-1484.
6. J. R. C. Guimares and J. C. Gomes, **Materials Science and Engineering** 39 (1979) 187-191.
7. K. Tsuzaki, S. Fukasaku, Y. Tomota and T. Maki, **Materials Transactions** JIM 32 (1991) 222-228.
8. Ch Maier , O. Blaschko and W. Pichl, **Physical Review** B 52 (1995) 9283-9290.
9. J. R. Yang, C. Y. Huang, W. H. Hsieh and C. S. Chiou, **Materials Transactions** JIM 37 (1996) 579-585.
10. X. Song, N. Gu and H. Peng, **Defect and Diffusion Forum** 148-149 (1997) 165-167.
11. M. C. Tsai, C. S.Chiou, J. S. Du and J. R. Yang, **Materials Science and Engineering** A332 (2002) 1-10.
12. H. K. D. H. Bhadeshia, **Materials Science and Engineering** A 378A (2004) 34-39.
13. J.P. McCaffrey and J. Hulse, **Micron** 29, (1998), 139-144.
14. M. J. Dickson, J. Appl. **Crystallography** 2 (1969) 176-180.
15. MTDATA, National Physical Laboratory, Teddington, London.
16. D. J. C. MacKay **Neural Computation** 4 (1992) 415-472.
17. H. K. D. H. Bhadeshia, **ISIJ International** 39 (1999) 966-979.

Originally published in Materials Science and Technology, 21 (2005) 1323-1328

www.ingentaconnect.com/content/maney/mst